

Controlling electron localization of H_2^+ by intense plasmon-enhanced laser fields

I. Yavuz¹, M. F. Ciappina², A. Chacón³, Z. Altun¹, and M. Lewenstein^{3,4}

¹*Marmara University, Physics Dep. 34722, Ziverbey, Istanbul, Turkey*

²*Max-Planck-Institut für Quantenoptik, Hans-Kopfermann-Strasse 1, D-85748 Garching, Germany*

³*ICFO-Institut de Ciències Fotòniques, The Barcelona Institute of Science and Technology, 08860 Castelldefels (Barcelona), Spain and*

⁴*ICREA-Institució Catalana de Recerca i Estudis Avançats, Lluís Companys 23, 08010 Barcelona, Spain*

(Dated: October 14, 2021)

We present a theoretical study of the wave packet dynamics of the H_2^+ molecular ion in plasmon-enhanced laser fields. Such fields may be produced, for instance, when metallic nano-structures are illuminated by a laser pulse of moderated intensity. Their main property is that they vary in space on nanometer scales. We demonstrate that the spatial inhomogeneous character of these plasmonic fields leads to an enhancement of electron localization, an instrumental phenomenon that controls molecular fragmentation. We suggest that the charge-imbalance induced by the surface-plasmon resonance near the metallic nano-structures is the origin of the increase in the electron localization.

PACS numbers: 42.65.Ky, 78.67.Bf, 32.80.Ee

I. INTRODUCTION

Studies of atomic and molecular quantum dynamics are in the center of interests of contemporary atomic, molecular and optical physics. There are various ways to induce such dynamics, but a very distinct one is to expose the atomic/molecular systems to an intense and coherent electromagnetic radiation. As a consequence of this coupling, new and diverse phenomena occur. Amongst the plethora of processes which take place, the two most prominent ones are the high-order harmonic generation (HHG) and the above-threshold ionization (ATI). They both lie at the core of the so-called attosecond physics [1, 2]. The quasi-classical picture of these two phenomena relies on the so-called three-step or simple man's model [3, 4]. Briefly, this approach can be summarized listing the subsequent steps: (i) tunnel ionization due to the intense and low frequency laser field; (ii) acceleration of the free electron by the laser electric field, and (iii) re-collision with the parent ion after the temporally oscillating laser electric field reverses the direction of the electronic motion. In HHG the electron recombines with the remaining ion-core and the excess of energy is converted into a high energy photon [2]. On the other hand, if the electron is re-scattered by the atomic potential, it gains even more kinetic energy and contributes to the high energy parts of the ATI spectrum [5].

Commonly, the laser ionization process is understood by invoking the quasi-static tunnel ionization picture. In this approach in every time (short) interval the laser electric field is considered as a static electric field. This assumption is valid for low photon frequencies – long wavelengths, and the atomic or molecular electron is considered to quickly tunnel out through the barrier created by the combined potentials of the laser electric field and the attractive Coulomb atomic/molecular potential. The main consequence of this description is that the ionization rate presents a maximum whenever the barrier

becomes the thinnest, which correlates with the electric field maxima. This prediction appears to be also valid in the so-called non-adiabatic tunnel ionization, i.e. when the laser electric field is considered to change significantly, while the electron is escaping from the attractive potential of the atomic or molecular core. For these cases the ionization rate exhibits a single maximum during each half-cycle of the laser electric field oscillation [6].

When molecules are used as driven media, the above cited assumptions should be revised, considering that there can be multiple bursts of ionization within a half-cycle of the laser electric field [7, 8]. By using different numerical models and simulations, it was confirmed that these bursts are related to the effect of transient electron localization (EL) at one of the heavy nuclei of the molecule on a sub-fs time scale [9–11]. Generally, a sub-cycle oscillation of the electron density occurs after the molecular ion has been stretched to intermediate internuclear distances, and it is due to a trapping of the electron population in a pair of so-called charge-resonance (CR) states [12, 13]. For the case of a simple H_2^+ molecular ion, they are the energetically lowest σ_g and σ_u states. It is likely, however, that both the multiple ionization bursts, and the CR appear in other more complex molecules as well. In addition, EL appears to be the responsible of the strongly enhanced ionization rate, observed for stretched molecules beyond its equilibrium internuclear separation [14], and, moreover, it was shown EL can be manipulated, joint with the control of photoabsorption/photodissociation, by using different alignment techniques (see e.g. [15]).

In the theoretical modeling of conventional strong laser-matter interaction, the main assumption is that both the laser electric field ($E(\mathbf{r}, t)$) and its vector potential associated ($A(\mathbf{r}, t)$) are spatially homogeneous in the region where the electron develops its motion and only their time dependence is considered, i.e. $E(\mathbf{r}, t) = E(t)$ and $A(\mathbf{r}, t) = A(t)$. This is a legitimate assumption since the fields change at most on the scale of the wavelength

(800 – 3000 nm), while the typical size of a laser focus is between several tens to a couple of hundreds microns (10^{-6} m). These scales have to be compared with the size of the electronic ground states (say of the order of Angstroms (10^{-10} m)), and the size of the typical electron excursions, estimated classically using $\alpha = E_0/\omega_0^2$; even these sizes remain sub-wavelength and do not reach more than tens of nm (10^{-9} m) for longer wavelengths and higher laser intensities (note that $\alpha \propto \lambda_0^2$, where λ_0 is the wavelength of the driven laser and $E_0 = \sqrt{I}$ where I is the laser intensity) [2]. On the contrary, the fields generated using surface plasmons are spatially dependent on a nanometer scale. By exploiting the surface plasmon resonance (SPR), locally enhanced electric field can be induced around gold bow-tie nano-antennas. The enhanced field boosts up the low incoming laser intensity, specified in the 10^{11} W cm $^{-2}$ range, by more than 30 dB, which becomes then strong enough to exceed the threshold laser intensity for HHG generation in noble gases [16]. The pulse repetition rate, typically in the MHz domain, remains unaltered without any extra pumping or cavity attachment; this is one of the main advantages of this setup. From a theoretical viewpoint, plasmonic fields open a wide range of possibilities to enhance and/or shape spectral and spatial properties of the incoming fields [17–20]. A peculiar property of this plasmonic fields is that the enhanced laser electric field is not spatially homogeneous, on the scales and in regions of comparable dimensions with the size of the electronic excursion α , where the electron dynamics takes place. Consequently, significant changes in the laser-matter processes arise.

There has been a remarkable theoretical activity on this subject recently [21–53]. In most of the contributions, however, only the HHG and ATI processes in atoms were studied and analyzed exclusively. Only recently investigations of HHG in simple molecules, H_2^+ , driven by plasmonic fields were presented [54, 55]. In the present paper we focus on the question to what extent plasmonic fields could configure a novel and reliable tool to control molecular dynamics, and in particular the electron localization (EL). As mentioned above, these fields are spatially inhomogeneous and thus they offer to our disposal a new degree of control, which could help us to obtain an even more precise manipulation of the electron and molecular dynamics at a sub-cycle time scale.

Our article is organized as follows. In Sec. II, we describe the methods, including here a brief description about the set up that could be utilized for the generation of plasmonic enhanced fields and its main characteristics. Once we have defined our theoretical model and observables of interest, we then analyze them and discuss their properties and implications in Sec. III. Finally, in Sec. IV, we end the paper with conclusions and a brief outlook.

II. METHODOLOGY

A. Field-enhancement by the nano-structure

A typical set up including both the metal bow-tie nano-antenna and the driven H_2^+ molecule is shown in Fig. 1 (for more details about the fabrication see e.g. [16]). The metal nano-structure takes the form of two triangular-shaped pads made of gold with a gap between their apexes (top panel). A planar substrate with a dielectric constant $\epsilon_s = 2.0$ supports them. In the diagram, h is the height, t is the thickness of the metal and g defines the gap between the tips. In the present simulations, we use $h = 100$ nm, $t = 40$ nm and $g = 20$ nm. We note that the chosen geometry parameters of the nano-antennae do not correspond to an optimum field-enhancement, i.e. the nano-antenna is not fully resonant with the laser wavelength, set at $\lambda = 800$ for the finite-difference time-domain (FDTD) simulations (see e.g. [23]), but these values are found to be sufficient to understand the underlying physics of the wave packet dynamics of the H_2^+ molecular ion near the metallic nano-structure. In order to mimic more realistic situations, the curvature radii of the tips are set to be 4 nm. The spatial profile of the field-enhancement around the bow-tie is determined using the MEEP code [56], that is based on the FDTD approach. The field-enhancement in the gap along the z -axis is shown in the bottom panel of Fig. 1, where the spatial profile is normalized to the intensity enhancement at the center ($z = 0$). We observe that the laser electric field peak amplitude is enhanced roughly by a factor of 2.5 near the metal tips compared with the center value, corresponding to a 4 dB of increase in the laser intensity.

B. Numerical solution of time-dependent Schrödinger equation (TDSE) for the H_2^+ molecule

The numerical solution of the TDSE for the interaction of a linearly polarized laser field with a H_2^+ molecule, in reduced dimensions, is considered as,

$$i \frac{d}{dt} \Psi(z, R, t) = \left[-\frac{1}{2} \frac{\partial^2}{\partial z^2} - \frac{1}{2\mu_p} \frac{\partial^2}{\partial R^2} + V_e(z, R) + V_n(R) + V_L(z, t) \right] \Psi(z, R, t). \quad (1)$$

where $\mu_p = m_p/2$ is the reduced-mass of the two nuclei. Here, the potentials $V_e(z, R)$ and $V_n(R)$ are the electron-nuclei attraction and nucleus-nucleus repulsion terms, respectively. The explicit forms of these potentials in reduced dimensions are given below [57]:

$$V_e(z, R) = -\frac{a}{\sqrt{(z + R/2)^2 + b(R)}} - \frac{a}{\sqrt{(z - R/2)^2 + b(R)}}, \quad (2)$$

and

$$V_n(R) = \frac{1}{R}. \quad (3)$$

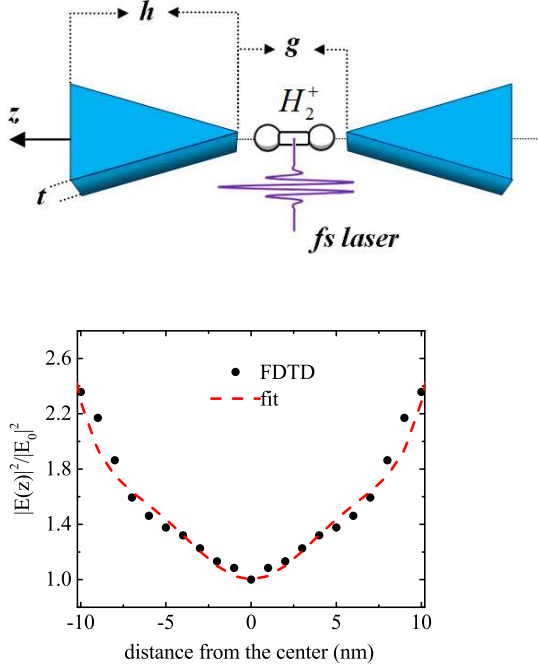


FIG. 1: (color online) Top: Typical geometry parameters of the bow-tie shaped gold nano-antennae considered in our study. Here, we take $h = 100$ nm, $t = 40$ nm and $g = 20$ nm. The curvature radii of the tips are taken as 4 nm. The bond distance R of the H_2^+ molecule is visually exaggerated for clarity. Bottom: The spatial profile of the field-enhancement in the gap, along z -axis, obtained from FDTD simulations. Circles are the actual enhancement determined by FDTD and solid line is a polynomial fitting, as described in the text. Note that, the laser electric field peak amplitude is enhanced roughly by a factor of 2.5 near the metals compared with the center value, corresponding to a 4 dB of increase in the laser intensity.

In Eq. (2) $a = 0.251$ is a scaling parameter and $b(R)$ is a function introduced to exactly reproduce the 3D potential energy curve of the $1\sigma_g$ state of the H_2^+ molecule. The laser-molecule interaction term $V_L(z, t)$ in the dipole approximation can be written as:

$$\begin{aligned} V_L(z, t) &= -zE(z, t) \\ &= -zE(t)[1 + s\kappa(z)]. \end{aligned} \quad (4)$$

where it is assumed that the laser electric field $E(z, t)$ is now function explicitly of both time and space. In Eq. (4) $\kappa(z) = \sum_i c_i z^i$ is a polynomial series that represents the functional form of the plasmonic field, determined by fitting it to the data obtained from FDTD simulations (see Fig. 1, bottom panel) and s is a switch function taking values $s = 0, 1$. s is used to turn the field inhomogeneity on or off, as discussed later. Note that the inter-nuclear axis of the H_2^+ molecule is placed as to coincide with the axis passing through the edges of the nano-structure element (see Fig. 1, top panel).

The field-free form of Eq. (1),

$$\left[-\frac{1}{2} \frac{\partial^2}{\partial z^2} - \frac{1}{2\mu_p} \frac{\partial^2}{\partial R^2} + V_e(z, R) + V_n(R) \right] \Psi(z, R) = E\Psi(z, R). \quad (5)$$

is numerically solved based on the Born-Oppenheimer (BO) approximation. When we apply the BO approximation to Eq. (5), its solution is expressed as follows:

$$\Psi(z, R, t = 0) = \phi_e(z, R)\psi_n(R) \quad (6)$$

where $\phi_e(z, R)$ is a set of electronic wavefunctions for fixed values of R and $\psi_n(R)$ is the nuclear wave function. Both $\phi_e(z, R)$ and $\psi_n(R)$ are calculated from the eigenvalue equations:

$$\left[-\frac{1}{2} \frac{\partial^2}{\partial z^2} + V_e(z, R) \right] \phi(z, R, t) = E_e(R)\phi(z, R, t), \quad (7)$$

and

$$\left[-\frac{1}{2\mu_p} \frac{\partial^2}{\partial R^2} + E_e(R) + V_n(R) \right] \psi(R) = E\psi(R), \quad (8)$$

respectively.

The field-free solutions of Eq. (7) and (8) for H_2^+ give an equilibrium bond distance $R = 2.0$ a.u. The ionization potential I_p at the equilibrium $1\sigma_g$ state is found to be $|E_e(R = 2.0)| = 30.0$ eV, i.e. the actual value I_p of the H_2^+ molecule is indeed reproduced.

The time-dependent part of the electric field in Eq. (4) is taken as $E(t) = E_0 f(t) \cos(\omega_0 t)$. E_0 and ω_0 are the peak amplitude [E_0 (a.u.) = $\sqrt{I/I_0}$] and $I_0 = 35.1$ PW cm^{-2}] and the frequency of the driving laser electric field, respectively. $f(t)$ is a flat-top, 10-cycles long pulse envelope with half-cycle ramp up/down (total time duration 27 fs). During the simulations both the electronic and nuclear wave functions are multiplied by mask functions of the form $\cos^{1/8}$ in each time step in order to avoid spurious reflections at the boundaries [58].

By using the time-dependent wave-function $\Psi(z, R, t)$ of Eq. (1) it is then possible to compute a set of physical quantities of interest, namely:

(i) the time-dependent norm $N(t)$

$$N(t) = \int_0^\infty dR \int_{-\infty}^\infty dz |\Psi(z, R, t)|^2, \quad (9)$$

(ii) the ionization probability $P_{ion}(t)$,

$$P_{ion}(t) = 1 - N(t), \quad (10)$$

(iii) the dissociation channels through upper $P_+(t)$ or lower $P_-(t)$ nuclei

$$P_\pm(t) = \int_{R_c}^\infty dR \int_0^{\pm z_c} dz |\Psi(z, R, t)|^2, \quad (11)$$

(iv) the dissociation probability $P_{dissoc}(t)$

$$P_{dissoc}(t) = P_+(t) + P_-(t), \quad (12)$$

and (v) the asymmetry parameter $A(t)$

$$A(t) = P_+(t) - P_-(t). \quad (13)$$

The integration limits in Eq. (11) R_c and z_c are taken as 10 a.u. The asymmetry parameter $A(t)$ determines the degree of localization in either of the heavy nuclei upon dissociation. Here, $A(t) > 0$ or $A(t) < 0$ refer to a high degree of localization on the upper or the lower nuclei, respectively. For $A(t) = 0$, the dissociative wave-packet is evenly distributed over both nuclei or no dissociation occur at all.

Finally, the time-dependent expectation value of the internuclear distance $R(t)$ is calculated by the following expression:

$$\langle R(t) \rangle = \frac{1}{N(t)} \int_0^\infty R dR \int_{-\infty}^\infty dz |\Psi(z, R, t)|^2. \quad (14)$$

This quantity allows us to monitor the time dynamics of the molecular dissociation.

III. RESULTS

In this section, we explore the influence of the spatial inhomogeneous character of the plasmonic field on the dissociation/ionization dynamics of H_2^+ molecular ion by comparing results for both conventional and spatial inhomogeneous fields. As stated otherwise, we consider that the centroid of H_2^+ coincides with the center of the gap of the metallic nano-structure, as shown in Fig. 1, and the molecule is initially in the ground electronic $1\sigma_g$ and vibrational $v = 0$ states.

Here, one can think the field spatial inhomogeneity as a potential landscape whose strength is enhanced as we move away from the gap center to the metallic surfaces (see Fig. 1). In contrast, an homogeneous field is independent of space, thus, constant in the region where the electron dynamics take place. In other words, the plasmonic character of the laser electric field is effective when the wave-packet is released from the bound state and spread across distant regions. Accordingly, there is a strong correlation between the ionization rate and the degree of field spatial inhomogeneity. On the other hand, since opposing charges are confined in opposing sides of the nano-structure due to SPR [16], freed electrons of target atoms/molecules would experience diverse (repulsive or attractive) forces depending on the direction of wave-packet's propagation.

Figures 2(a)-2(g) show time-dependent wave packet properties of the H_2^+ molecular ion in a laser field with and without a spatial inhomogeneous character ($s = 0$ and $s = 1$, respectively). The laser intensity and the wavelength of the laser field are fixed at $I = 300 \text{ TW/cm}^2$

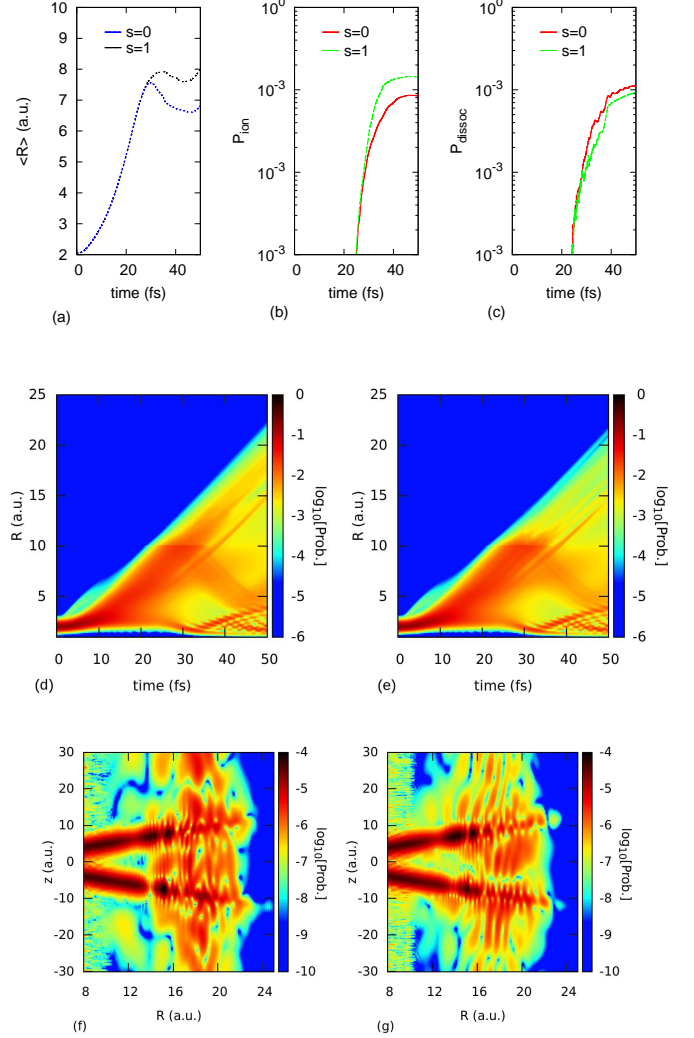


FIG. 2: (color online) (a) Temporal variation of R , i.e. $\langle R(t) \rangle$, (b) ionization probability and (c) dissociation probability of the H_2^+ for $s = 0$ and $s = 1$ (see Eq. (4) for more details). (Center) Time dependence of R -resolved probability distribution $|\Psi(R, t)|^2$ of H_2^+ for $s = 0$ (left) and $s = 1$ (right). (f) and (g) show the snapshots of the wave-packet distributions of $s = 0$ and $s = 1$, when the wave-packet is relaxed for a sufficient amount of time after the pulse ends. The laser intensity is $I = 300 \text{ TW cm}^{-2}$ and $\lambda = 800 \text{ nm}$. The pulse comprises 10 total cycles (27 fs) and we use a flat-top pulse envelope with half-cycle ramp up/down.

($3 \times 10^{14} \text{ W/cm}^2$) and $\lambda = 800 \text{ nm}$, respectively. Firstly, in Fig. 2(a) we show the time-dependent variation of R , i.e. $\langle R(t) \rangle$. Since, the laser field is switched off at $t = 27 \text{ fs}$, it is clear that the plasmonic-laser field is effective when the wave-packet begins to relax resulting in a slightly higher bond elongation. It is also evident from Fig. 2(b) that the field inhomogeneity emerges when ionization reaches a certain level (again almost immediately after the pulse is over), which is $P_{ion} \sim 10^{-2}$. In addition, the ionization probability increases roughly by a factor of two after reaching a, sort of, limiting value. However,

as shown in Fig. 2(c), the dissociation probability is only slightly lower for $s = 1$ (inhomogeneous) than for $s = 0$ (homogeneous), suggesting a more direct electron ionization channel.

Figures 2(d)-2(e) show the time-variation of the nuclear probability density for $s = 0$ and $s = 1$, respectively. In the bound region (i.e. for $R < 10$ a.u.), $s = 0$ and $s = 1$ have similar profiles, however the dissociation region (i.e. when $R > 10$ a.u.) is slightly more occupied in the case of $s = 0$, consistent with Fig. 2(c).

Finally, Figs. 2(f)-2(g) show the electron-nuclear coordinate maps when the wave-packets are relaxed for a sufficient amount of time after the pulse is turned-off. Comparing with the homogeneous case, and in the dissociation region, in particular for $R > 14$ a.u., the wave-packet is much more localized on both nuclei for the case of the plasmonic field. This is a significant outcome showing the control the plasmonic character of the field has on EL. In order to quantify this last asseveration, using Eq. (13), we find that, after the wave-packet is relaxed, the asymmetry parameter is $A = -7.2 \times 10^{-4}$ for $s = 0$ and $A = 1.3 \times 10^{-2}$ for $s = 1$. Thus the asymmetry (localization) for the case of the plasmonic field is roughly 20 times larger than the conventional case.

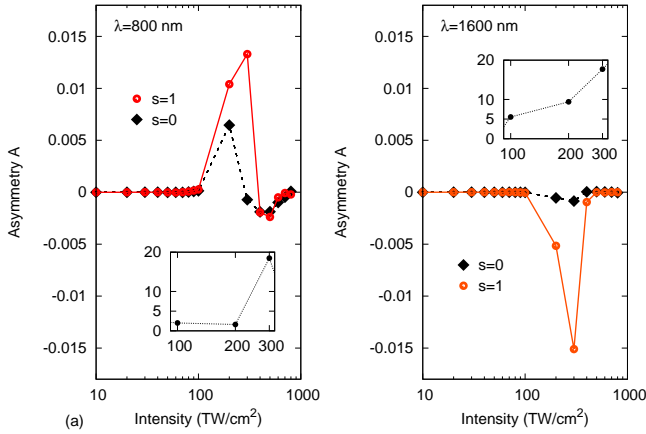


FIG. 3: (color online) Variation of the asymmetry parameter ($A = P_+ - P_-$) parameter of H_2^+ as a function of plasmonic field-intensity for $s = 0$ and $s = 1$ (see Eq. (4) for details). A values are calculated after pulse is turned-off and then the system is left to relax for a sufficient amount of time. We have performed calculations for two different wavelengths; (a) $\lambda = 800$ nm and (b) $\lambda = 1600$ nm. Insets show the absolute asymmetry parameter enhancement, i.e. the absolute ratio between A of $s = 1$ and $s = 0$, in the region $I = 100 - 300 \text{ TW}/\text{cm}^2$. The temporal and spatial profile of the laser electric field is the same as in Fig. 1.

The intensity dependence of the *relaxed* asymmetry parameter A of wave packet dissociation at $\lambda = 800$ and 1600 nm is shown in Fig. 3. For $s = 0$, A is enhanced in the intensity region $100 - 300 \text{ TW}/\text{cm}^2$ for both $\lambda = 800$ and 1600 nm. For weak fields, A is nearly zero due to the low wave packet dissociation rates. For strong intensities,

however, direct wave packet ionization may occur, which also reduces dissociation. Thus, there is an intermediate intensity region ($100 - 300 \text{ TW}/\text{cm}^2$ in our case) such that dissociation reaches a maximum, so is the asymmetry parameter A . On the other hand, comparing with that of $\lambda = 800$ nm, A is lower in the intermediate region ($100 - 300 \text{ TW}/\text{cm}^2$) for $\lambda = 1600$ nm. This is attributed to faster vibrational motions induced by longer wavelengths, causing an increase in the wave packet ionization. When the molecule is placed in a plasmon-enhanced laser field ($s = 1$), the asymmetry parameter A is nearly zero in the weak and strong intensity regions, similar to the case of $s = 0$. On the other hand, in the intermediate intensity region, A is dramatically enhanced for both $\lambda = 800$ and 1600 nm. In numbers, for plasmonic fields at $\sim I = 200 - 300 \text{ TW}/\text{cm}^2$ the asymmetry parameter A is enhanced by a factor of $5 \sim 20$ compared with the conventional case for both $\lambda = 800$ nm (see Fig. 3(a)) and $\lambda = 1600$ nm (see Fig.

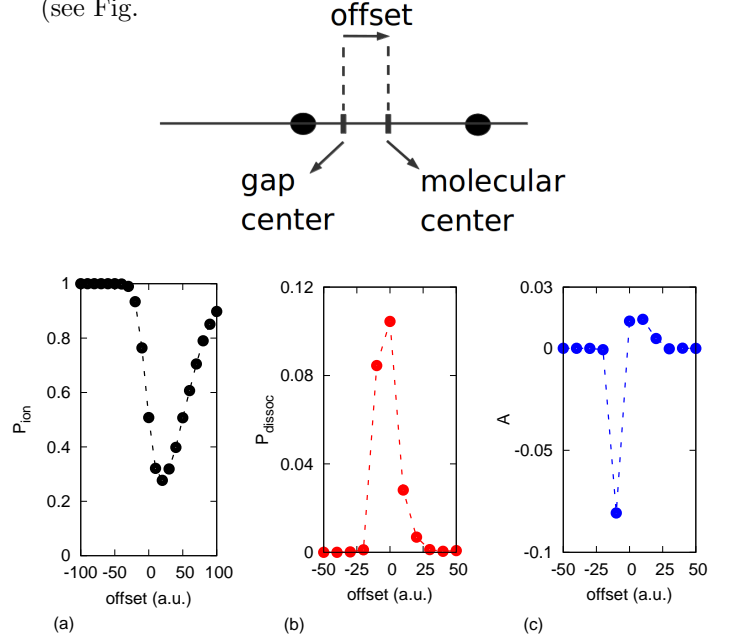


FIG. 4: (color online) Top: An illustration showing the gap center of the nano-structure element, molecular center (centroid) of H_2^+ and offset with respect to the gap center. Full circles illustrates the positions of the nuclei. (a) ionization probability, (b) dissociation probability and (c) asymmetry parameter, $A = P_+ - P_-$, as a function of the centroid offset. P_{ion} , P_{dissoc} and A are calculated after pulse is turned-off and then the system is left to relax for a sufficient amount of time. The laser field parameters are the same as in Fig. 2.

We argue that a charge-imbalance, in the nano-gap region, induced by the plasmonic field is the responsible for the dramatic enhancement in the asymmetry parameter A . So far, we assume that the centroid of the molecule and gap center coincides, but in a real experiment we could have molecules randomly distributed in the nano-gap region. Thus one could ask, what happens if we displace the molecule from the gap center to the left or right regions along the z -axis, where positive or negative

charges dominate? In order to gain further understanding in the control of dissociation asymmetry by the plasmonic field, we simulate the wave packet dynamics of H_2^+ molecule by displacing its centroid coordinates along the z -axis of the nano-structure, as illustrated in Fig. 4 (top). In a region where positive or negative charges dominate, the wave packet might be steered further by attractive or repulsive forces (towards or away from the metallic surface), respectively.

Figures 4(a)-4(c) show the ionization (Fig. 4(a)) and dissociation probabilities (Fig. 4(b)) and the asymmetry parameter A (Fig. 4(c)) as a function of centroid offset with respect to the gap center. Our results show that there is a clear and strong interplay between ionization, dissociation and the resulting asymmetry parameter A . The asymmetry in ionization probability is clearly visible in Fig. 4(a). In the negative offset region, a steep increase in P_{ion} within $-40 < \text{offset} < 0$ is observed and full ionization occurs beyond this point. In the positive offset region, on the other hand, P_{ion} increases gradually. These results suggest that for the negative offset region the ionized wave packet is pulled towards the metallic surfaces, while in the positive region is pulled backwards, thus suppressing ionization as much as possible. After a certain point, however, the excursion of the wave packet reaches the metallic surface causing electron absorptions by the metallic surfaces [30, 59].

Wavepacket's dissociation probability P_{dissoc} , on the contrary, reaches a maximum for zero offset and gradually diminishes in both regions due to the increase of P_{ion} . The dissociation asymmetry parameter A is larger in the gap center region and maximum, in amplitude, when the offset is ≈ -10 a.u. Positive values of A in the positive offset region and negative values of A in the negative offset region is evident due to an unevenly distribution of charges in the nano-structure region. In other words, positive offset is causing EL in the upper nuclei, while the negative offset in the lower one, respectively.

IV. CONCLUSIONS AND OUTLOOK

We have studied electron localization (EL) in H_2^+ molecules driven by intense plasmonic fields. These fields are not spatially homogeneous in the region where the electron wave packet dynamics takes place and, as a consequence, are thus able to modify substantially the observables. To illustrate this fact we have solved the TDSE in reduced dimensions, including both the electron and nuclear dynamics. This model was proven to be suitable for the computation of both electron and nuclear related quantities.

We have shown that the spatial inhomogeneous character of the laser electric field allows us to enhance the localization of the electron in one of the two heavy ions and given physical grounds for this behavior. This enhancement can be modified, for instance, by engineering the geometry of the metal nano-structure.

Furthermore, with our model we can monitor the dissociation dynamics of the H_2^+ molecule as a function of the position with respect to the center of the gap between the bow-ties. This analysis is instrumental in order to perform realistic predictions.

The utilization of plasmonic fields could open the pathway to perform control of the EL and molecular dissociation at a more advanced level.

V. ACKNOWLEDGMENT

I.Y. and Z.A. acknowledge support from BAPKO of MU. Calculations are performed at the Simulations and Research Lab, Physics Department of MU. A.C. and M.L. acknowledge the Spanish MINECO project FOQUS (FIS2013-46768-P), the Catalan AGAUR project SGR 874, EU project QUIC, and ERC AdG OSYRIS.

-
- [1] P. B. Corkum and F. Krausz, *Nature Phys.* **3**, 381 (2007).
 - [2] F. Krausz and M. Ivanov, *Rev. Mod. Phys.* **81**, 163 (2009).
 - [3] P. B. Corkum, *Phys. Rev. Lett.* **71**, 1994 (1993).
 - [4] M. Lewenstein, P. Balcou, M. Y. Ivanov, A. L'Huillier, and P. B. Corkum, *Phys. Rev. A* **49**, 2117 (1994).
 - [5] D. B. Milošević, G. G. Paulus, D. Bauer, and W. Becker, *J. Phys. B* **39**, R203 (2006).
 - [6] G. L. Yudin and M. Y. Ivanov, *Phys. Rev. A* **64**, 013409 (2001).
 - [7] N. Takemoto and A. Becker, *Phys. Rev. Lett.* **105**, 203004 (2010).
 - [8] N. Takemoto and A. Becker, *J. Comp. Phys.* **134**, 074309 (2011).
 - [9] I. Kawata, H. Kono, and Y. Fujimura, *J. Comp. Phys.* **110**, 11152 (1999).
 - [10] F. He, A. Becker, and U. Thumm, *Phys. Rev. Lett.* **101**, 213002 (2008).
 - [11] N. Takemoto and A. Becker, *Phys. Rev. A* **84**, 023401 (2011).
 - [12] R. S. Mulliken, *J. Comp. Phys.* **7**, 20 (1939).
 - [13] L. Pauling, *Proc. Nat. Acad. Sci. USA* **25**, 577 (1939).
 - [14] T. Seideman, M. Y. Ivanov, and P. B. Corkum, *Phys. Rev. Lett.* **75**, 2819 (1995).
 - [15] H. Stapelfeldt and T. Seideman, *Rev. Mod. Phys.* **75**, 543 (2003).
 - [16] S. Kim, J. Jin, Y.-J. Kim, I.-Y. Park, Y. Kim, and S.-W. Kim, *Nature* **453**, 757 (2008).
 - [17] I.-Y. Park, S. Kim, J. Choi, D.-H. Lee, Y.-J. Kim, M. F. Kling, M. I. Stockman, and S.-W. Kim, *Nat. Photonics* **5**, 677 (2011).
 - [18] J. Choi, S. Kim, I.-Y. Park, D.-H. Lee, S. Han, and S.-W. Kim, *New J. Phys.* **14**, 103038 (2012).
 - [19] N. Pfullmann, C. Waltermann, M. Noack, S. Rausch, T. Nagy, C. Reinhardt, M. Kovačev, V. Knittel, R. Bratschkitsch, D. Akemeier, et al., *New J. Phys.* **15**, 093027 (2013).

- (2013).
- [20] I.-Y. Park, J. Choi, D.-H. Lee, S. Han, S. Kim, and S.-W. Kim, *Ann. Phys. (Berlin)* **525**, 87 (2013).
 - [21] A. Husakou, S.-J. Im, and J. Herrmann, *Phys. Rev. A* **83**, 043839 (2011).
 - [22] A. Husakou, F. Kelkensberg, J. Herrmann, and M. J. J. Vrakking, *Opt. Exp.* **19**, 25346 (2011).
 - [23] M. F. Ciappina, S. S. Aćimović, T. Shaaran, J. Biegert, R. Quidant, and M. Lewenstein, *Opt. Exp.* **20**, 26261 (2012).
 - [24] M. F. Ciappina, J. Biegert, R. Quidant, and M. Lewenstein, *Phys. Rev. A* **85**, 033828 (2012).
 - [25] T. Shaaran, M. F. Ciappina, and M. Lewenstein, *Phys. Rev. A* **86**, 023408 (2012).
 - [26] M. F. Ciappina, J. A. Pérez-Hernández, T. Shaaran, J. Biegert, R. Quidant, and M. Lewenstein, *Phys. Rev. A* **86**, 023413 (2012).
 - [27] T. Shaaran, M. F. Ciappina, and M. Lewenstein, *J. Mod. Opt.* **86**, 1634 (2012).
 - [28] I. Yavuz, E. A. Bleda, Z. Altun, and T. Topcu, *Phys. Rev. A* **85**, 013416 (2012).
 - [29] J. A. Pérez-Hernández, M. F. Ciappina, M. Lewenstein, L. Roso, and A. Zair, *Phys. Rev. Lett.* **110**, 053001 (2013).
 - [30] I. Yavuz, *Phys. Rev. A* **87**, 053815 (2013).
 - [31] M. F. Ciappina, J. A. Pérez-Hernández, T. Shaaran, L. Roso, and M. Lewenstein, *Phys. Rev. A* **87**, 063833 (2013).
 - [32] T. Shaaran, M. F. Ciappina, R. Guichard, J. A. Pérez-Hernández, L. Roso, M. Arnold, T. Siegel, A. Zair, and M. Lewenstein, *Phys. Rev. A* **87**, 041402(R) (2013).
 - [33] M. F. Ciappina, T. Shaaran, and M. Lewenstein, *Ann. Phys.* **525**, 97 (2013).
 - [34] T. Shaaran, M. F. Ciappina, and M. Lewenstein, *Phys. Rev. A* **87**, 053415 (2013).
 - [35] M. F. Ciappina, T. Shaaran, R. Guichard, J. A. Pérez-Hernández, L. Roso, M. Arnold, T. Siegel, A. Zair, and M. Lewenstein, *Las. Phys. Lett.* **10**, 105302 (2013).
 - [36] M. F. Ciappina, J. A. Pérez-Hernández, T. Shaaran, M. Lewenstein, M. Krüger, and P. Hommelhoff, *Phys. Rev. A* **89**, 013409 (2014).
 - [37] M. F. Ciappina, J. A. Pérez-Hernández, T. Shaaran, and M. Lewenstein, *Eur. Phys. J. D* **68**, 172 (2014).
 - [38] M. F. Ciappina, J. A. Pérez-Hernández, and M. Lewenstein, *Comp. Phys. Comm.* **185**, 398 (2015).
 - [39] M. F. Ciappina, J. A. Pérez-Hernández, L. Roso, A. Zair, and M. Lewenstein, *J. Phys.: Conf. Ser.* **601**, 012001 (2015).
 - [40] A. Husakou and J. Herrmann, *Phys. Rev. A* **90**, 023831 (2014).
 - [41] H. Ebadi, *Phys. Rev. A* **89**, 053413 (2014).
 - [42] B. Fetić, K. Kalajdžić, and D. B. Milošević, *Ann. Phys.* **525**, 107 (2012).
 - [43] J. Luo, Y. Li, Z. Wang, Q. Zhang, and P. Lu, *J. Phys. B* **46**, 145602 (2013).
 - [44] L. Feng, M. Yuan, and T. Chu, *Phys. Plasmas* **20**, 122307 (2013).
 - [45] Z. Wang, P. Lan, J. Luo, L. He, Q. Zhang, and P. Lu, *Phys. Rev. A* **88**, 063838 (2013).
 - [46] J. Luo, Y. Li, Z. Wang, L. He, Q. Zhang, P. Lan, and P. Lu, *Phys. Rev. A* **89**, 023405 (2014).
 - [47] L. He, Z. Wang, Y. Li, Q. Zhang, P. Lan, and P. Lu, *Phys. Rev. A* **88**, 053404 (2013).
 - [48] C. Zhang, C. Liu, and Z. Xu, *Phys. Rev. A* **88**, 035805 (2013).
 - [49] J. Luo, Y. Li, Z. Wang, Q. Zhang, P. Lan, and P. Lu, *J. Opt. Soc. Am. B* **30**, 2469 (2013).
 - [50] X. Cao, S. Jiang, C. Yu, Y. Wang, L. Bai, and R. Lu, *Opt. Exp.* **22**, 26153 (2014).
 - [51] Z. Wang, L. He, J. Luo, P. Lan, and P. Lu, *Opt. Exp.* **22**, 25909 (2014).
 - [52] L. Feng and H. Liu, *Phys. Plasmas* **22**, 013107 (2015).
 - [53] C. Yu, Y. Wang, X. Cao, S. Jiang, and R. Lu, *J. Phys. B* **47**, 225602 (2015).
 - [54] I. Yavuz, Y. Tikman, and Z. Altun, *Phys. Rev. A* **92**, 023413 (2015).
 - [55] L. Feng, *Phys. Rev. A* **92**, 053832 (2015).
 - [56] A. F. Oskooi, D. Roundy, M. Ibanescu, P. Bermel, J. Joannopoulos, and S. G. Johnson, *Comp. Phys. Comm.* **181**, 687 (2010).
 - [57] K. C. Kulander, F. H. Mies, and K. J. Schafer, *Phys. Rev. A* **53**, 2562 (1996).
 - [58] J. L. Krause, K. J. Schafer, and K. C. Kulander, *Phys. Rev. A* **45**, 4998 (1992).
 - [59] A. Husakou, S.-J. Im, and J. Herrmann, *Phys. Rev. A* **83**, 043839 (2011).